# Fetch Relations for Wind-Generated Waves as a Function of Wind-Stress Scaling

WILL PERRIE AND BECHARA TOULANY

*Physical and Chemical Sciences, Scotia–Fundy Region, Department of Fisheries and Oceans, Bedford Institute of Oceanography, Dartmouth, Nova Scotia, Canada*

(Manuscript received 29 October 1989, in final form 26 February 1990)

ABSTRACT

We present the variation that results when fetch relations for wind-generated wave spectra are scaled by the friction velocity component in the dominant wave direction rather than the magnitude of the friction velocity, using the data collected during the Canadian Atlantic Storms Program (CASP). The effects of three possible drag coefficients are considered: the usual constant drag coefficient, the open-ocean long fetch drag coefficient, and finally, the wave age dependent drag coefficient for growing waves recently measured by Smith and Anderson in HEXOS.

Contributions to the correlation coefficients for dimensionless variables due to both scaling variables and dimensional variables are computed. We find that the friction velocity component in the dominant wave direction rather than the friction velocity magnitude should be used as the scaling variable. The self-correlation introduced to the correlation coefficients is then less than that resulting from the friction velocity magnitude.

Balance relations among physical fetch relations support this conclusion and imply that the wave age dependent drag coefficient for growing waves is the appropriate drag coefficient to use in scaling variables. We generalize Snyder et al.'s parameterization of the wind input energy and derive a functional form for Phillips' equilibrium range $\alpha$-function.

## 1. Introduction

Implications of an $f^{-4}$ power law for the equilibrium range of high frequencies in the energy spectrum for wind-generated surface gravity waves were recently explored by Resio and Perrie (1989). They discussed spectra described by the JONSWAP parameterization as given by Hasselmann et al. (1973),

$$E(f) = \frac{\tilde{\alpha} g^2 f^{-5}}{(2\pi)^4} \exp\left(-1.25 \frac{f_m^4}{f^4}\right) \gamma^{\Xi} \quad (1.1)$$

where $f_m$ is the frequency of the spectral peak, $\tilde{\alpha}$ is a proportionality coefficient specified by the high frequency range ($f > 2.5 f_m$) of the spectrum and exponent $\Xi$ is given by

$$\Xi = \exp\left[-\frac{1}{2}\left(\frac{f - f_m}{\sigma f_m}\right)^2\right]. \quad (1.2)$$

Directional spectra may be represented by (1.1) using a spreading function $\mathcal{J}(f, \theta)$:

$$\mathcal{J}(f, \theta) = \Omega(f)\left(\cos\tfrac{1}{2}(\theta - \theta_0)\right)^{\mathcal{P}(f)} \quad (1.3)$$

where $\theta$ is the wave direction, $\theta_0(f)$ is the mean wave direction at $f$, $\mathcal{P}(f)$ is a function of frequency $f$, and the normalization coefficient $\Omega(f)$ satisfies

$$\int_{-\pi}^{\pi} \Omega(f)\left(\cos\tfrac{1}{2}\theta\right)^{\mathcal{P}(f)} d\theta = 1. \quad (1.4)$$

They also considered spectra with an $f^{-4}$ equilibrium range at high frequencies represented by

$$E(f, \theta) = \tilde{\alpha} \mathcal{U} g f^{-4} \psi\left(\frac{f}{f_m}\right) \mathcal{J}(\theta - \theta_0) \quad (1.5)$$

where $\psi$ is a nondimensional shape function modeling the forward face, peak and high frequency regions of the spectrum. The scaling in (1.5) uses wind speed $\mathcal{U}$ at a reference height rather than the phase velocity $\mathcal{C}_p$ at the peak frequency of the wave spectrum as suggested by Donelan et al. (1985).

Assuming the JONSWAP fetch relations, Resio and Perrie (1989) derived transfer rates for energy and momentum from wind to waves in the case of generating windsea. These were used as constraints on the functional form assumed by the input of energy from wind to windsea in parameterizations suggested by Snyder et al. (1981), Plant (1982) and Phillips (1985). A partitioning of spectral energy, as in the original JONSWAP study, and a parameterization of fluxes within the spectrum was seen to lead to a functional form for $\tilde{\alpha}$.

We suggest that different results would follow had the scaling been done differently and the CASP dataset

*Corresponding author address:* Dr. Will Perrie, Bedford Institute of Oceanography, P.O. Box 1006, Dartmouth, Nova Scotia, B2Y 4A2 Canada.

of Dobson et al. (1989) been used. We discuss the meaning of alternate scalings in section 2, and apply these to the CASP dataset in section 3. The spurious effects that poorly chosen scaling variables can introduce to the analysis are dealt with in section 4. Proper scaling variables, consistent fetch relations, formulations for $\tilde{\alpha}$ and for wind input energy, are presented in section 5.

## 2. Nondimensional scaling

For many years it has been common to scale total energy $E_0$ in terms of wind speed $\mathcal{U}$ at some reference height such as 10 m (Hasselmann et al. 1973). Following Kitaigorodskii (1962), Janssen et al. (1987) and Dobson and Toulany (1989) we may also scale $E_0$ using friction velocity $\mathcal{U}_*$, expressed as

$$E_0^* = E_0 g^2 / \mathcal{U}_*^4 \tag{2.1}$$

where $\mathcal{U}_*$ is related to a drag coefficient $C_d$ by the relation

$$\mathcal{U}_* = \mathcal{U}\sqrt{C_d}. \tag{2.2}$$

As noted by Donelan et al. (1985), waves are not strictly locally generated, but instead are the net result of an evolution along their entire fetch. Therefore, if the gradient of fetch about the wind direction is large, the wave direction is biased towards long fetch where a lower generating force due to wind input $\mathcal{U}\cos\Delta\theta(f_m)$, is more than compensated by the longer fetch over which it operates. We are therefore motivated to introduce $\mathcal{U}_{*c}$, the friction velocity component in the direction of the waves at the peak frequency $f_m$. An alternate form for dimensionless total energy is

$$E_0^{*c} = E_0 g^2 / \mathcal{U}_{*c}^4. \tag{2.3}$$

Friction velocity magnitude $\mathcal{U}_*$ is related to $\mathcal{U}_{*c}$ by the relation

$$\mathcal{U}_{*c} = \mathcal{U}_* \cos(\Delta\theta(f_m)) \tag{2.4}$$

where $\Delta\theta(f_m)$ is the difference between the 10 m wind direction $\theta_w$, and the mean wave direction $\theta_0(f_m)$ at $f_m$. A complete account of the determination of $\Delta\theta(f_m)$, the separation of swell from offshore waves propagating along a specific fetch and the generation situation of the waves is given in Dobson et al. (1989).

Clearly we could define dimensionless fetch or dimensionless peak frequency in the same manner as (2.1) or (2.3) for total energy. For example, dimensionless fetch $X^*$ scaled using $\mathcal{U}_*$ may be specified by

$$X^* = Xg/\mathcal{U}_*^2 \tag{2.5}$$

whereas scaled by $\mathcal{U}_{*c}$, dimensionless fetch $X^{*c}$ is

$$X^{*c} = Xg/\mathcal{U}_{*c}^2. \tag{2.6}$$

There are several ways to specify drag coefficient $C_d$. We use $C_{d1}$ to denote the constant drag coefficient,

$$C_{d1} = 1.3 \times 10^{-3}. \tag{2.7}$$

Smith (1988) measured the drag coefficient for open-ocean long-fetch conditions from his stable tower at the mouth of Halifax Harbour and found that at reference height 10 m, $C_d$ depended on $\mathcal{U}$ and $\Delta T$, the difference between water and air temperatures. We denote this drag coefficient $C_{d2}$ where

$$C_{d2} = C_d[\mathcal{U}, \Delta T]. \tag{2.8}$$

In the recent Humidity EXperiment Over the Sea (HEXOS), Smith and Anderson (1989) measured the drag coefficient for young generating waves and related it to wave age $\mathcal{C}_p/\mathcal{U}_c$, expressed in terms of $\mathcal{U}_c$, the component wind velocity in the direction of the waves at $f_m$. This can be termed "component wave age." Denoting this drag coefficient $C_{d3}$, Smith (personal communication) has recently suggested the parameterization

$$C_{d3} = \begin{cases} C_{d2} + (1.51 - 1.87\mathcal{C}_p/\mathcal{U}_c) \times 10^{-3}, \\ \qquad \text{when} \quad 0 < \mathcal{C}_p/\mathcal{U}_c < 0.81 \\ C_{d2}, \quad \text{otherwise} \end{cases} \tag{2.9}$$

where corrections for sensor tilt have been made to the data. We emphasize that this formulation will need further minor corrections when all the data from HEXOS has received a final analysis. As this assumes neutral stability, $C_{d3}$ should generally be appropriate for growing wind-generated waves when we correct our data to neutrally stable conditions,

## 3. CASP growth curves

Recent analysis of data collected during the Canadian Atlantic Storm Program (CASP) by Dobson et al. (1989), found good agreement with earlier experiments such as Donelan et al. (1985) in Lake Ontario and JONSWAP. New insight was gained into the wind profile for generating waves in fetch-limited situations. Specifically, data collected by Smith and McPherson (1987) verified earlier modeling of the planetary boundary layer by Taylor and Lee (1984), that as fetch increases from the shoreline and waves are initiated and grow, the change in roughness at the boundary layer leads to an increase in the wind speed at a reference height. The wind profile is a function of fetch and falls within the envelope defined by the two curves of Fig. 1. These are generated by considering different upstream roughnesses for the shoreline. The upper curve corresponds to marsh, whereas the lower curve corresponds to forest. These are shown to present the two extremes that Taylor and Lee (1984) give as a function of the terrain onshore from the experiment.

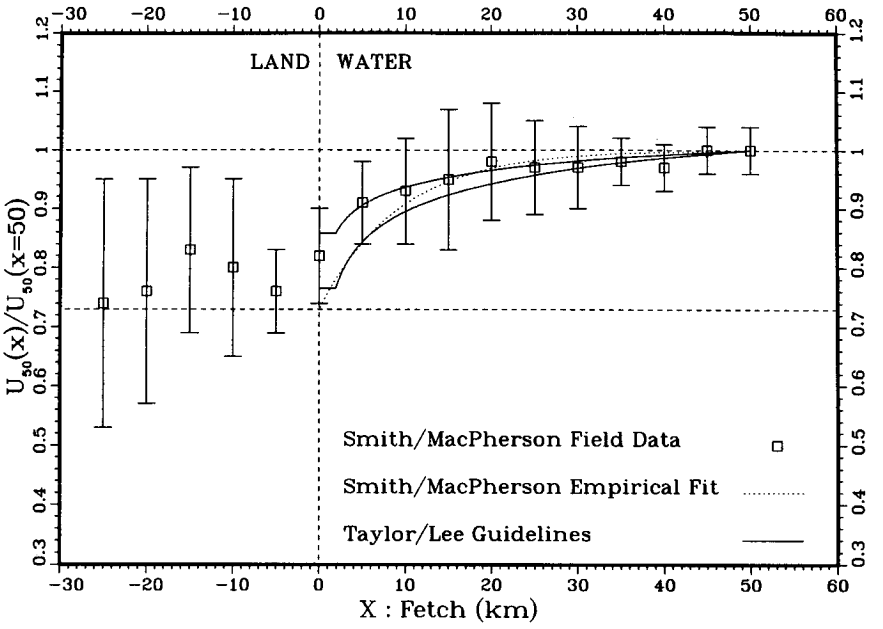


FIG. 1. The wind profile as a function of fetch from Taylor and Lee (1984) for upstream roughness lengths such as marsh 0.07 m, the upper curve ——, forest and low terrain 1 m, the lower curve ——, compared to aircraft winds collected by Smith and MacPherson (1987) at 50 m elevation - - -, showing standard deviation error bars.

The actual Taylor and Lee (1984) model for the wind profile that we used falls between these two extremes and follows the Smith and McPherson (1987) empirical curve well.

In JONSWAP and Donelan et al. (1985), dimensional wave variables were scaled by in situ wind. In the present analysis, wave measurements at each buoy were scaled by the wind, linearly averaged along the fetch from the shore to each of the wave buoys exactly following the procedure of Dobson et al. (1989). This represents the ability of the waves to "remember" the wind all along the fetch. Scaling by the average wind along the fetch is certainly only one way to represent this memory. As mentioned in Dobson et al. (1989), the greatest discrepancy between linearly averaged wind and in situ wind occurs not at the shortest fetches but at the intermediate fetches, at about 15 km, when the fetch-averaged wind is about 0.9 of the in situ wind. Linearly averaged wind is the same as in situ wind for fetches that approach zero or infinity.

It was seen in JONSWAP, Donelan et al. (1985), and Dobson et al. (1989) that dimensionless variables such as peak frequency, total energy and wave age, can be parameterized by simple power-law relations. In terms of dimensionless fetch $X^*$, we present these as

$$E_0^* = \mathcal{E}(X^*)^{\epsilon} \tag{3.1}$$

$$f_m^* = \mathcal{F}(X^*)^{\phi} \tag{3.2}$$

$$\alpha^* = \mathcal{A}(X^*)^{a} \tag{3.3}$$

and alternately in terms of inverse wave age $\mathcal{U}_*/\mathcal{C}_p$:

$$E_0^* = \mathbf{E}[\mathcal{U}_*/\mathcal{C}_p]^{\epsilon} \tag{3.4}$$

$$X^* = \mathbf{X}[\mathcal{U}_*/\mathcal{C}_p]^{\xi} \tag{3.5}$$

$$\alpha^* = \mathbf{A}[\mathcal{U}_*/\mathcal{C}_p]^{\zeta}. \tag{3.6}$$

When scaling uses the friction velocity component in the direction of the waves $\mathcal{U}_{*c}$, the corresponding nondimensional fetch $X^{*c}$ relations are

$$E_0^{*c} = \mathcal{E}(X^{*c})^{\epsilon} \tag{3.7}$$

$$f_m^{*c} = \mathcal{F}(X^{*c})^{\phi} \tag{3.8}$$

$$\alpha^{*c} = \mathcal{A}(X^{*c})^{a} \tag{3.9}$$

and in terms of inverse wave age $\mathcal{U}_{*c}/\mathcal{C}_p$:

$$E_0^{*c} = \mathbf{E}[\mathcal{U}_{*c}/\mathcal{C}_p]^{\epsilon} \tag{3.10}$$

$$X^{*c} = \mathbf{X}[\mathcal{U}_{*c}/\mathcal{C}_p]^{\xi} \tag{3.11}$$

$$\alpha^{*c} = \mathbf{A}[\mathcal{U}_{*c}/\mathcal{C}_p]^{\zeta}. \tag{3.12}$$

Dimensionless peak frequency $f_m^*$ in (3.2) is computed by scaling peak frequency $f_m$ with friction velocity $\mathcal{U}_*$,

$$f_m^* = f_m \mathcal{U}_*/g \tag{3.13}$$

and similarly in (3.8), $f_m^{*c}$ is scaled using $\mathcal{U}_{*c}$.

We evaluate the various forms of $\tilde{\alpha}$ from the energy formulation (1.5),

$$\alpha^* = \frac{(2\pi)^3}{g\mathcal{U}_*} \frac{1}{(f_N - 1.5f_m)} \times \int_{1.5f_m}^{f_N} f^4 E(f) \exp\left(\frac{f_m^4}{f^4}\right) df \quad (3.14)$$

where $f_N$ is nyquist (0.64 Hz for the CASP dataset). Scaling with respect to $\mathcal{U}_{*c}$ leads to an analogous relation for $\alpha^{*c}$.

The variation in scatter in the total energy fetch relations (3.1) and (3.7), that results from scaling in terms of $\mathcal{U}_*$ and $\mathcal{U}_{*c}$ and the drag coefficients $C_{d1}$, $C_{d2}$ and $C_{d3}$, is shown in Figs. 2a–f. This is for waves associated with winds whose mean directions were within a ±15° window from normal to the shoreline as seen from a given buoy. The corresponding families of curves are presented in Figs. 3a and 3b for a ±15° and a ±30° window from normal to the shoreline, respectively. The slopes, intercepts and correlation coefficients $R$, corresponding to these curves and to the scatter of Figs. 2a–f, are written in Table 1. For a given drag coefficient, scaling by $\mathcal{U}_*$ results in the same correlation coefficient as scaling by $\mathcal{U}_{*c}$. Generally $C_{d3}$ results in better (that is, closer to unity) correlation coefficients than $C_{d2}$, which in turn does better than $C_{d1}$.

The slopes, intercepts, and correlation coefficients for the $f_m$ variation with $X$ in (3.2) and (3.8); the $\tilde{\alpha}$ variation with $X$ in (3.3) and (3.9); the $E_0$ variation with $\mathcal{U}_c/\mathcal{C}_p$ in (3.4) and (3.10); the $X$ variation with $\mathcal{U}_c/\mathcal{C}_p$ in (3.5) and (3.11); and finally, the $\tilde{\alpha}$ variation with $\mathcal{U}_c/\mathcal{C}_p$ in (3.6) and (3.12) are also presented in Table 1. Results corresponding to the ±30° window are given in Table 2.

The variation of $f_m$ with $X$ and $\mathcal{U}_c/\mathcal{C}_p$ follows the trend set by the variation of $E_0$ with $X$. Scaling by $\mathcal{U}_*$ results in the same correlation coefficient as scaling by $\mathcal{U}_{*c}$, for a given drag coefficient. Generally scaling with $C_{d3}$ results in better correlation coefficients than scaling with $C_{d2}$, which in turn does better than $C_{d1}$. This trend is repeated in the variation of $E_0$ with $\mathcal{U}_c/\mathcal{C}_p$ except that some preference is shown for scaling by

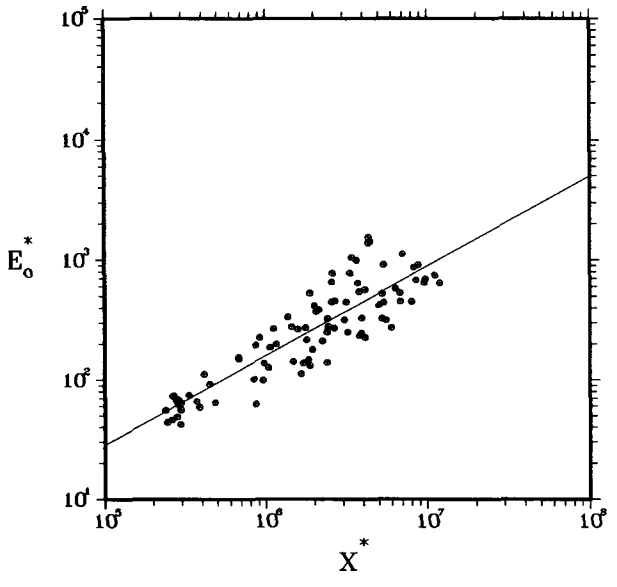


FIG. 2a. Dimensionless energy $E_0^*$ as a function of dimensionless fetch $X^*$ using $C_{d1}$ and $\mathcal{U}_*$ scaling, for waves associated with winds whose directions were within a ±15° window from normal to the shoreline. Least squares fit is indicated by (——).

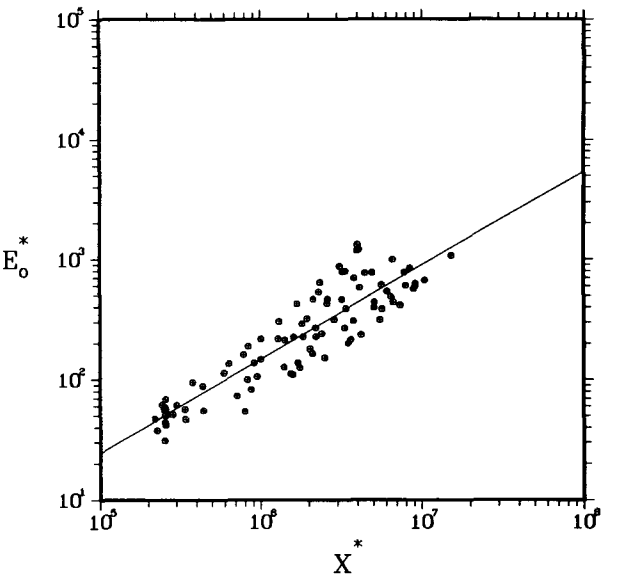


FIG. 2b. As in Fig. 2a but using $C_{d2}$ and $\mathcal{U}_*$ scaling.

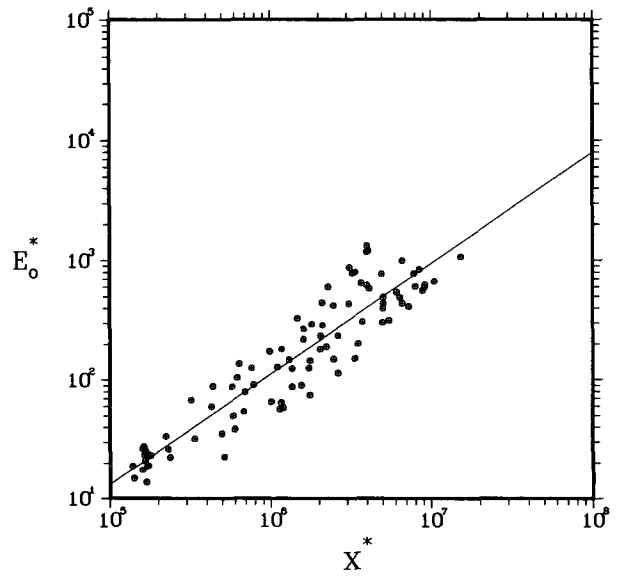


FIG. 2c. As in Fig. 2a but using $C_{d3}$ and $\mathcal{U}_*$ scaling.

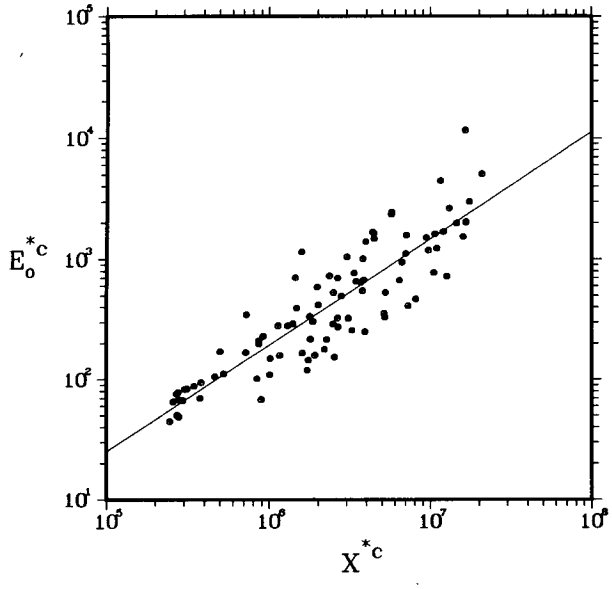


FIG. 2d. As in Fig. 2a but using $C_{d1}$ and $\mathcal{U}_{*c}$ scaling.

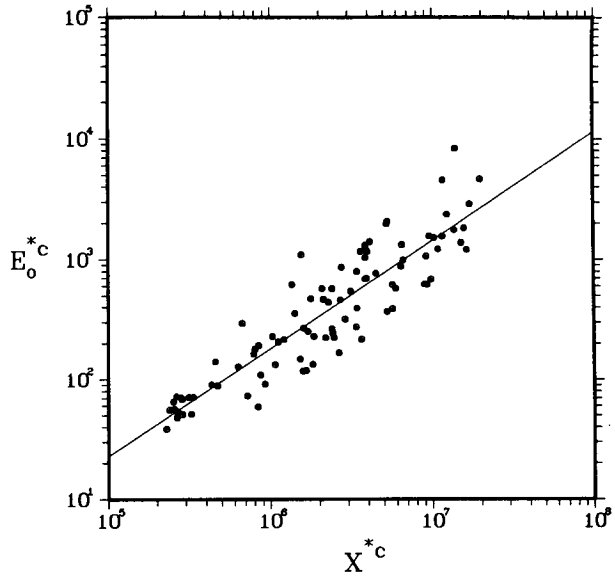


FIG. 2e. As in Fig. 2a but using$C_{d2}$ and $\mathcal{U}_{*c}$ scaling.

$\mathcal{U}_{*c}$ rather than by $\mathcal{U}_*$. The variations of $\tilde{\alpha}$ with $X$ and $\mathcal{U}_c/\mathcal{C}_p$ have better correlation coefficients when scaling uses $\mathcal{U}_{*c}$ rather than $\mathcal{U}_*$ for a given drag coefficient. In these computations, $C_{d3}$ surpasses $C_{d2}$, which in turn does better than $C_{d1}$.

The significance of slanting fetch with respect to the CASP data was considered by Dobson et al. (1989). Results obtained when the wind direction $\theta_w$ is within ±30° from normal to the mean shoreline, were generally consistent with JONSWAP fetch curves, which analyzed waves associated with winds whose mean directions were also within a ±30° window from normal to the shoreline. Narrowing this window to ±15° or ±5°, or using $\mathcal{U}_c$ as a scaling variable, led to relations that agree with the higher resolution results of Donelan et al. (1985).

We suggest that the ±30° window allows contamination from slanting fetch waves. This increases the computed growth in wave energy relative to the growth seen when a narrower window is specified. Furthermore, using the wind velocity component in the dominant wave direction (at $f_m$) enhances the computed growth in wave energy relative to that seen when wind speed magnitude is used as the scaling variable.

However, variations in exponent $e$ from different experiments are difficult to explain. For example, we found that $e$ is 0.88 scaling with $\mathcal{U}_{*c}$ and drag coefficient $C_{d1}$ as opposed to 0.75 scaling with $\mathcal{U}_*$ and $C_{d1}$, assuming the ±15° window. Using the in situ scalar wind speed as scaling variable in the analysis of the JONSWAP data, Hasselmann et al. (1973) found $e$ to be 1.0 or slightly lower in Phillips' (1977) reanalysis, for waves associated with the ±30° window. In either case this exceeds the 0.88 or 0.75 reported in Table 1, whereas Donelan et al. (1985) used the in situ wind velocity component in the dominant wave direction $\mathcal{U}_c$ as scaling variable and obtained $e$ very close to 0.75.

In an attempt to bring these results together, Walsh et al. (1989) derived the direction of maximum wave energy and period growth for slanting fetch situations. They suggested that $e$ and $f$ are coupled and should satisfy

$$\frac{f - f_0}{f_0 + 2f_0 f} = \frac{e - e_0}{e_0 - e_0(e/2)} \tag{3.15}$$

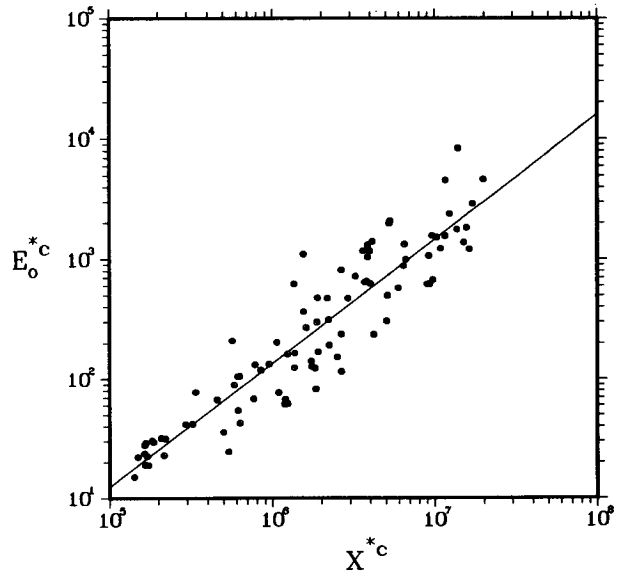


FIG. 2f. As in Fig. 2a but using $C_{d3}$ and $\mathcal{U}_{*c}$ scaling.

TABLE 1. The exponents, coefficients and correlation coefficients $R$, corresponding to the fetch relations of (3.1)–(3.12) as a function of drag coefficient and wind stress scaling for waves associated with winds within a ±15° window to normal from the shoreline.

| | Scaling with $\mathcal{U}_*$ | | | Scaling with $\mathcal{U}_{*c}$ | | |
|---|---|---|---|---|---|---|
| | $C_{d1}$ | $C_{d2}$ | $C_{d3}$ | $C_{d1}$ | $C_{d2}$ | $C_{d3}$ |
| $e$ | 0.75 ± .09 | 0.78 ± .08 | 0.93 ± .08 | 0.88 ± .10 | 0.90 ± .09 | 1.04 ± .09 |
| $\mathcal{E} \times 10^4$ | 52.8 | 30.5 | 3.02 | 9.57 | 7.16 | 0.816 |
| $R$ | 0.88 | 0.90 | 0.93 | 0.88 | 0.90 | 0.92 |
| $f$ | −0.24 ± .02 | −0.24 ± .02 | −0.28 ± .02 | −0.27 ± .03 | −0.27 ± .02 | −0.30 ± .02 |
| $\mathcal{F} \times 10$ | 2.91 | 3.30 | 5.50 | 4.56 | 4.86 | 7.71 |
| $R$ | −0.92 | −0.93 | −0.94 | −0.91 | −0.92 | −0.94 |
| $a$ | 0.06 ± .05 | 0.08 ± .05 | 0.13 ± .05 | 0.12 ± .05 | 0.13 ± .05 | 0.17 ± .05 |
| $\mathcal{A} \times 10^2$ | 6.25 | 4.87 | 2.15 | 2.97 | 2.57 | 1.23 |
| $R$ | 0.24 | 0.30 | 0.49 | 0.41 | 0.45 | 0.59 |
| $\epsilon$ | −3.21 ± .19 | −3.22 ± .17 | −3.37 ± .13 | −3.32 ± .13 | −3.31 ± .12 | −3.44 ± .10 |
| $\mathbf{E} \times 10^2$ | 3.19 | 3.04 | 1.89 | 2.58 | 2.61 | 1.69 |
| $R$ | −0.96 | −0.97 | −0.98 | −0.98 | −0.98 | −0.99 |
| $\xi$ | −3.63 ± .32 | −3.58 ± .29 | −3.23 ± .24 | −3.09 ± .29 | −3.11 ± .27 | −2.91 ± .22 |
| $\mathbf{X} \times 10^2$ | 0.733 | 0.854 | 2.54 | 2.85 | 2.72 | 5.32 |
| $R$ | −0.92 | −0.93 | −0.94 | −0.91 | −0.92 | −0.94 |
| $\zeta$ | −0.39 ± .19 | −0.43 ± .18 | −0.55 ± .15 | −0.59 ± .16 | −0.60 ± .16 | −0.67 ± .13 |
| $\mathbf{A} \times 10^2$ | 4.90 | 4.32 | 2.96 | 2.93 | 2.85 | 2.26 |
| $R$ | −0.40 | −0.45 | −0.63 | −0.62 | −0.63 | −0.67 |

where $f_0$ and $e_0$ are reference values for $f$ and $e$. Assuming −0.23 and 0.76 for $f_0$ and $e_0$ from Donelan et al. (1985), Walsh et al. (1989) approximate this as

$$e + 4f = -0.16 \qquad (3.16)$$

which also satisfies our ±15° window results when $\mathcal{U}_{*c}$ and $C_{d3}$ are used as scaling variables.

In Fig. 4 we compare (3.15), as plotted by Walsh et al. (1989) using $f_0$ and $e_0$ from Donelan et al. (1985), to what we achieve from the possible scalings recorded in Tables 1 and 2. When $f = -0.30$ and $e = 1.04$ the agreement is striking, and supports using $\mathcal{U}_{*c}$ and $C_{d3}$ as scaling variables. Also plotted are the results of Hasselmann et al. (1973), Phillips (1977), Liu and Ross (1980), Donelan et al. (1985) and Walsh et al. (1989). It is worth reiterating that the determination of (3.15)

TABLE 2. As in Table 1 but for winds within a ±30° window.

| | Scaling with $\mathcal{U}_*$ | | | Scaling with $\mathcal{U}_{*c}$ | | |
|---|---|---|---|---|---|---|
| | $C_{d1}$ | $C_{d2}$ | $C_{d3}$ | $C_{d1}$ | $C_{d2}$ | $C_{d3}$ |
| $e$ | 0.80 ± .06 | 0.85 ± .06 | 0.99 ± .06 | 1.04 ± .08 | 1.06 ± .08 | 1.17 ± .07 |
| $\mathcal{E} \times 10^4$ | 21.0 | 9.35 | 1.02 | 0.848 | 0.621 | 0.095 |
| $R$ | 0.87 | 0.88 | 0.91 | 0.87 | 0.88 | 0.91 |
| $f$ | −0.25 ± .02 | −0.26 ± .02 | −0.29 ± .02 | −0.31 ± .02 | −0.32 ± .02 | −0.34 ± .02 |
| $\mathcal{F} \times 10$ | 3.61 | 4.31 | 7.20 | 8.87 | 9.41 | 13.9 |
| $R$ | −0.90 | −0.91 | −0.93 | −0.89 | −0.90 | −0.92 |
| $a$ | 0.07 ± .04 | 0.10 ± .05 | 0.15 ± .04 | 0.16 ± .04 | 0.17 ± .04 | 0.21 ± .04 |
| $\mathcal{A} \times 10^2$ | 4.80 | 3.03 | 1.43 | 1.50 | 1.17 | 6.22 |
| $R$ | 0.21 | 0.29 | 0.44 | 0.44 | 0.47 | 0.59 |
| $\epsilon$ | −3.19 ± .13 | −3.25 ± .13 | −3.36 ± .10 | −3.35 ± .08 | −3.36 ± .08 | −3.45 ± .06 |
| $\mathbf{E} \times 10^2$ | 3.18 | 2.60 | 1.80 | 2.27 | 2.16 | 1.57 |
| $R$ | −0.96 | −0.96 | −0.98 | −0.99 | −0.99 | −0.99 |
| $\xi$ | −3.30 ± .22 | −3.21 ± .20 | −2.96 ± .16 | −2.55 ± .18 | −2.56 ± .17 | −2.50 ± .14 |
| $\mathbf{X} \times 10^2$ | 2.13 | 2.85 | 6.26 | 15.6 | 15.1 | 18.8 |
| $R$ | −0.90 | −0.91 | −0.93 | −0.89 | −0.90 | −0.92 |
| $\zeta$ | −0.42 ± .16 | −0.53 ± .15 | −0.61 ± .12 | −0.65 ± .11 | −0.69 ± .11 | −0.72 ± .09 |
| $\mathbf{A} \times 10^2$ | 4.13 | 2.94 | 2.34 | 2.32 | 2.06 | 1.81 |
| $R$ | −0.34 | −0.44 | −0.57 | −0.63 | −0.65 | −0.73 |

in Fig. 3 is not absolute, but simply the result of assuming that Donelan et al (1985) were correct in parameterizing in terms of $\mathcal{U}_c$ because $\mathcal{U}_c$ worked well with their Lake Ontario data and the radar data of Walsh et al. (1989). Interestingly, our values of $f$ and $e$ have a variation that is greater than the other five experiments collectively. The growth rates seem almost continuously adjustable and depend on the scaling and the method of analysis. It is impressive that all $(-f, e)$ points lie very close to a line parallel to the straight line (3.16), compared to the results obtained by Hasselmann et al. (1973), Phillips (1977), Liu and Ross (1980).

To clarify the role of fetch-dependence in the wind speed $\mathcal{U}$ and the drag coefficient $C_d$ in Fig. 4, we rewrite the total energy fetch relation (3.7) and the peak frequency fetch relation (3.8) in terms of dimensional variables,

$$E_0 = \mathcal{E}\,\frac{(\mathcal{U}\cos\Delta\theta(f_m))^{4-2e}C_d{}^{2-e}}{g^{2-e}}\,X^e \qquad (3.17)$$

$$f_m = \mathcal{F}\,\frac{g^{1+f}}{(\mathcal{U}\cos\Delta\theta(f_m))^{1+2f}C_d{}^{0.5+f}}\,X^f. \qquad (3.18)$$

We suggest that $\Delta\theta(f_m)$ is a function of fetch. At small fetch, $\Delta\theta(f_m)$ tends to zero because the propagation direction of young waves is near that of the wind. Long fetch within the CASP wave buoy array favours increased $\Delta\theta(f_m)$ because the fetch gradient about the wind direction is large. A lower generating force due to $\mathcal{U}\cos\Delta\theta(f_m)$ is balanced by a relatively longer fetch

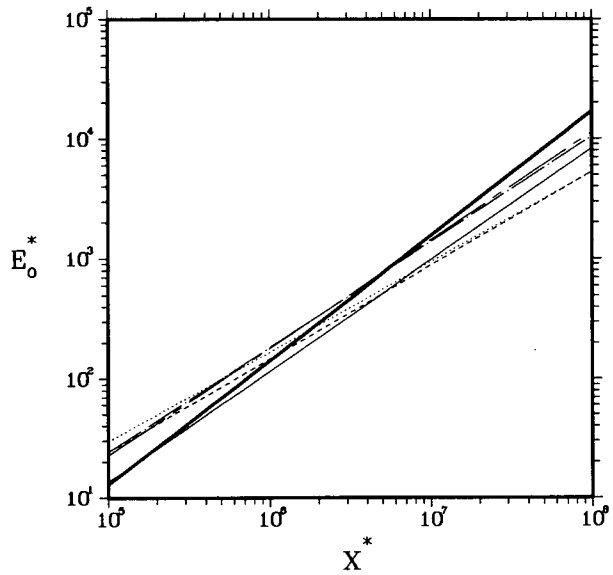


FIG. 3a. The family of curves for total energy as a function of fetch. The scaling is in terms of $\mathcal{U}_*$ and the drag coefficients $C_{d1}$ for dotted curve, $C_{d2}$ for dashed curve, $C_{d3}$ for thin solid curve, and in terms of $\mathcal{U}_{*c}$ and drag coefficients $C_{d1}$ for dot-dashed curve, $C_{d2}$ for short-long dashed curve and $C_{d3}$, for heavy solid curve; for waves associated with winds within ±15° from normal to the shoreline.

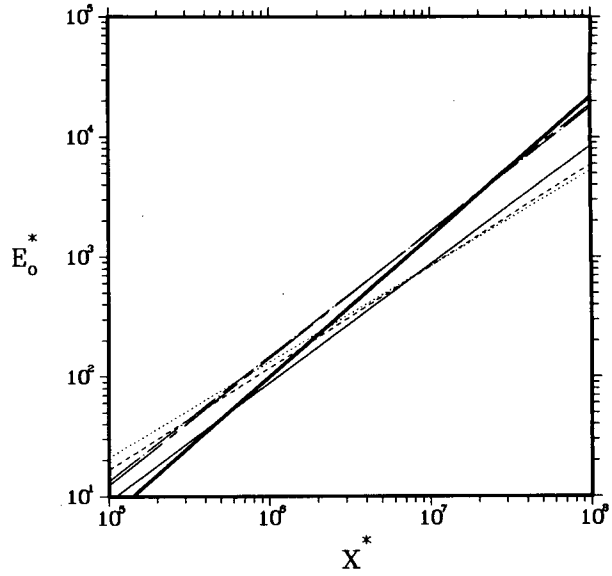


FIG. 3b. As in Fig. 3a for a window of ±30°.

associated with differing wind and wave directions (Donelan et al. 1985). The cumulative effect of combining observations from various days, fetches, wind speeds and directions is increased slopes in Figs. 4a and 3b and exponents $e$ in Tables 1 and 2, compared scaling by the scalar wind speed.

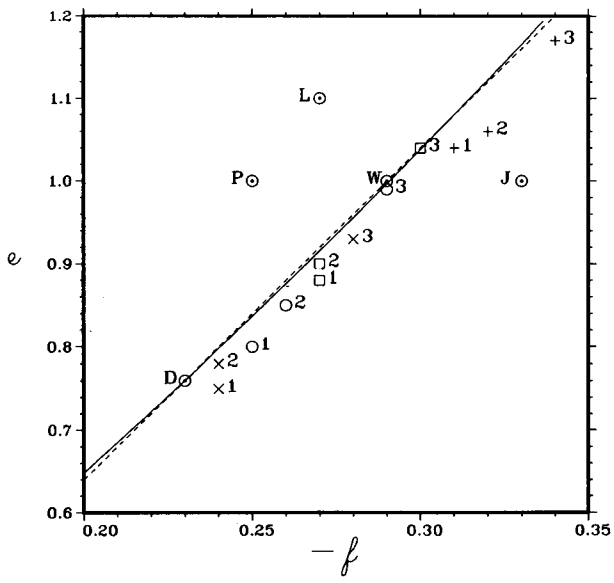


FIG. 4. Comparison of the coupling relation for $f$ and $e$ (3.15) assuming Donelan et al. (1985)'s reference $f_0$ and $e_0$ (solid), to $e + 4f = -0.16$ (dashed). Coordinates $(-f, e)$ from CASP are denoted (×) scaling with $\mathcal{U}_*$, (□) scaling with $\mathcal{U}_{*c}$, for the ±15° window, (○) scaling with $\mathcal{U}_*$, and (+) scaling with $\mathcal{U}_{*c}$ for the ±30° window. Numbers 1, 2 and 3 indicate scaling with drag coefficients $C_{d1}$, $C_{d2}$ and $C_{d3}$. Letters D, J, L, P and W are for Donelan et al. (1985), JONSWAP, Liu and Ross (1980), Phillips (1977) and Walsh et al. (1989).

Only data for which $\mathcal{U} \geq 5$ m s$^{-1}$ were considered for Figs. 2a–e and 3a–b. The variation of $C_{d2}$ with $\mathcal{U}$ for a given $\Delta T$ (the difference in temperature between water and air) is shown in Fig. 5 from Smith (1988). Assuming constant $\Delta T$, $C_{d2}$ should therefore increase as waves are generated at the shoreline and propagate offshore, in conjunction with the increase in $\mathcal{U}$ presented in Fig. 1 and the analysis of Smith and McPherson (1987) and Taylor and Lee (1984). We show $\Delta T$ for the CASP data in Fig. 6, measured as the difference in temperature between the water at the seaward end of the wave buoy array and the air at the shoreline. During situations when waves are propagating offshore, the wind direction is 340° true ±15° or ±30°, depending on the window, and $\Delta T$ varies from +15° to −5°C. The true $\Delta T$ is actually less than the values shown in Fig. 6 and decreases as distance from the shoreline increases and the water warms the air during offshore situations. Therefore, the dominating effect is that the drag coefficient $C_{d2}$ decreases with fetch and both $e$ and $f$ increase compared to scaling with $C_{d1}$. Furthermore, an explicit decrease in drag coefficient with increasing $c_p/\mathcal{U}_c$, as seen in $C_{d3}$ specified by (2.9), insures that $e$ and $f$ increase dramatically compared to scaling with $C_{d1}$.

To explain why our $(-f, e)$ points appear to spread out along a line in Fig. 4, we consider the variation of wave steepness, written as $E_0^{1/2}k_m$, with fetch. From (3.7) and (3.8), it follows that

$$E_0^{1/2}k_m = 4\pi^2 \mathcal{J}^2 \mathcal{E}^{1/2} (X^{*c})^{(4f+e)/2} \tag{3.19}$$

or in terms of dimensional variables

$$E_0^{1/2}k_m = 4\pi^2 \mathcal{J}^2 \mathcal{E}^{1/2} \left( \frac{Xg \cos^2 \Delta\theta(f_m)}{\mathcal{U}^2 C_d} \right)^{(4f+e)/2}. \tag{3.20}$$

The exponent $(4f + e)/2$ on the right side of this equation is small. Walsh et al. (1989) found that it is −0.08. Our $(-f, e)$ values in Fig. 3 lie along a line

$$e + 4f = -0.19 \tag{3.21}$$

parallel to (3.16) and the correlation coefficient is 0.99.

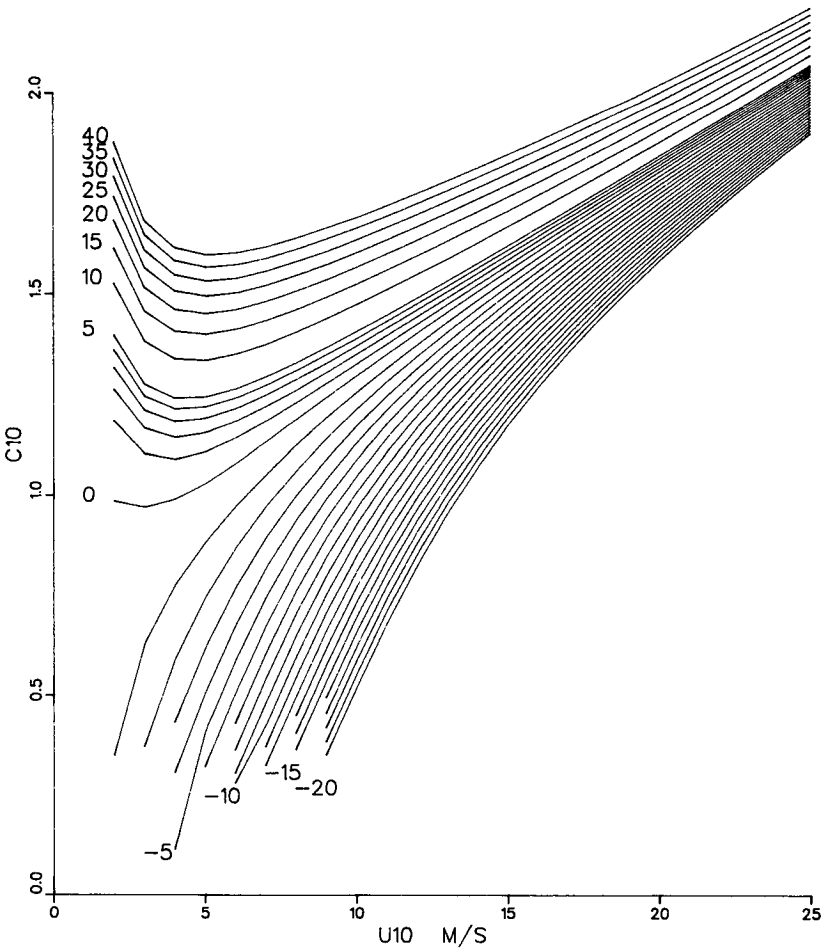


FIG. 5. Variation of drag coefficient $C_{d2}$ ($\times 10^3$) at 10 m with wind speed for sea-air potential virtual temperature differences of −20° to +40°, from Smith (1988).

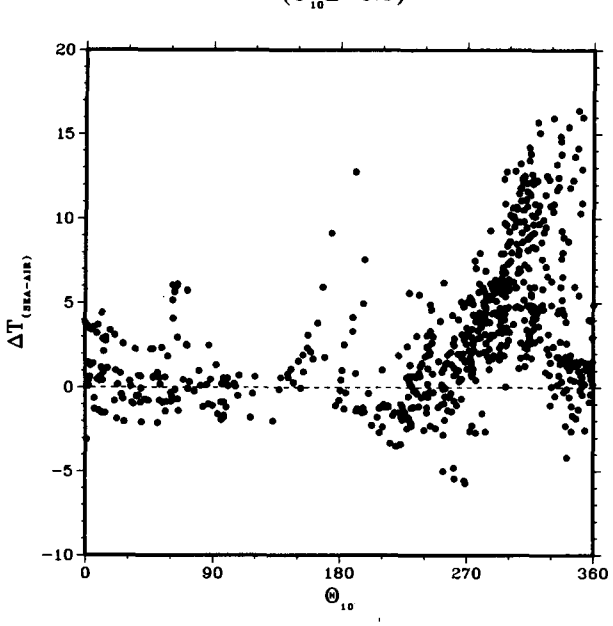


FIG. 6. Variation in the difference in temperature between the water at the seaward end of the wave buoy array and the air at the shoreline, with wind direction for the CASP data.

Wave steepness is therefore almost invariant with respect to fetch, regardless of the analysis that is applied. Fetch dependence within scaling variables $\mathcal{U}_{*c}$ and $C_d$ or the $\pm 15°$ or $\pm 30°$ window is relatively quite minor. The great range of growth rates along (3.21) reflect the dominance of this constraint.

## 4. Statistical implications of curve fitting and scaling self-correlation

There are two concerns that must be dealt with in discussing the scaling used to find relationships among dimensionless variables as we are doing in this paper. First, how do we know that the suggested scaling is ultimately the "best" or most correct? Is it simply that the associated correlation coefficient is highest or is it motivated by the most cogent physical arguments? Second, are we introducing any spurious self-correlation by using scaling variables that have a common factor, as in the manner in which we compute dimensionless total energy and fetch in (2.1) and (2.5)?

Suppose we have a dataset of dimensional variables denoted $\mathcal{X}(i)$ and $\mathcal{Y}(i)$ and we scale them by $\mathcal{u}(i)$ and $\mathcal{v}(i)$ to form dimensionless variables $\tilde{\mathcal{X}}(i)$ and $\tilde{\mathcal{Y}}(i)$ where

$$\left.\begin{aligned}\tilde{\mathcal{X}}(i) &= \mathcal{u}(i)\mathcal{X}(i)\\ \tilde{\mathcal{Y}}(i) &= \mathcal{v}(i)\mathcal{Y}(i)\end{aligned}\right\}. \tag{4.1}$$

We are really working with $\log\mathcal{X}$ and $\log\mathcal{Y}$ in deriving the power-law relations of (3.1)–(3.12) because we assume a linear relation between the logarithms of dimensionless variables of the form

$$\log\tilde{\mathcal{Y}} = a\log\tilde{\mathcal{X}} + \mathcal{l}. \tag{4.2}$$

The slope $\alpha$ in (4.2) is given by

$$\alpha = R_{\tilde{\mathcal{X}}\tilde{\mathcal{Y}}}[\mathrm{var}(\log\tilde{\mathcal{Y}})/\mathrm{var}(\log\tilde{\mathcal{X}})]^{1/2} \tag{4.3}$$

where $R_{\tilde{\mathcal{X}}\tilde{\mathcal{Y}}}$ is the correlation coefficient $R(\log\tilde{\mathcal{X}}, \log\tilde{\mathcal{Y}})$ between $\log\tilde{\mathcal{Y}}$ and $\log\tilde{\mathcal{X}}$, defined as

$$R_{\tilde{\mathcal{X}}\tilde{\mathcal{Y}}} \equiv \frac{\mathrm{cov}(\log\tilde{\mathcal{X}}, \log\tilde{\mathcal{Y}})}{[\mathrm{var}(\log\tilde{\mathcal{X}})\,\mathrm{var}(\log\tilde{\mathcal{Y}})]^{1/2}} \tag{4.4}$$

in terms of the usual relation for covariance,

$$\mathrm{cov}(\tilde{\mathcal{X}}, \tilde{\mathcal{Y}}) \equiv \langle(\tilde{\mathcal{X}} - \langle\tilde{\mathcal{X}}\rangle)(\tilde{\mathcal{Y}} - \langle\tilde{\mathcal{Y}}\rangle)\rangle \tag{4.5}$$

ensemble mean,

$$\langle\mathcal{X}\rangle \equiv \frac{1}{N}\sum_{i=1}^{N}\mathcal{X}_i \tag{4.6}$$

and variance

$$\mathrm{var}(\mathcal{X}) = \mathrm{cov}(\mathcal{X}, \mathcal{X}) \tag{4.7}$$

Following Jenkins and Watts (1968) and Kenny (1982), the correlation coefficient between $\log\tilde{\mathcal{Y}}$ and $\log\tilde{\mathcal{X}}$ is

$$R(\log\tilde{\mathcal{X}}, \log\tilde{\mathcal{Y}}) = \frac{R(\log\mathcal{X}, \log\mathcal{Y}) + \frac{\mathcal{S}_v}{\mathcal{S}_y}R(\log\mathcal{X}, \log\mathcal{v}) + \frac{\mathcal{S}_u}{\mathcal{S}_x}R(\log\mathcal{Y}, \log\mathcal{u}) + \frac{\mathcal{S}_u\mathcal{S}_v}{\mathcal{S}_x\mathcal{S}_y}R(\log\mathcal{u}, \log\mathcal{v})}{\left[1 + \frac{\mathcal{S}_u^{\,2}}{\mathcal{S}_x^{\,2}} + 2\frac{\mathcal{S}_u}{\mathcal{S}_x}R(\log\mathcal{X}, \log\mathcal{u})\right]^{1/2}\left[1 + \frac{\mathcal{S}_v^{\,2}}{\mathcal{S}_y^{\,2}} + 2\frac{\mathcal{S}_v}{\mathcal{S}_y}R(\log\mathcal{Y}, \log\mathcal{v})\right]^{1/2}} \tag{4.8}$$

where for example,

$$\mathcal{S}_x^{\,2} = \mathrm{var}(\log\mathcal{X}). \tag{4.9}$$

This relation may also be written as

$$R_{\tilde{\mathcal{X}}\tilde{\mathcal{Y}}} = \frac{R_{\mathcal{X}\mathcal{Y}} + \frac{\mathcal{S}_v}{\mathcal{S}_y}R_{\mathcal{X}\mathcal{v}} + \frac{\mathcal{S}_u}{\mathcal{S}_x}R_{\mathcal{Y}\mathcal{u}} + \frac{\mathcal{S}_u\mathcal{S}_v}{\mathcal{S}_x\mathcal{S}_y}R_{\mathcal{u}\mathcal{v}}}{\left[1 + \frac{\mathcal{S}_u^{\,2}}{\mathcal{S}_x^{\,2}} + 2\frac{\mathcal{S}_u}{\mathcal{S}_x}R_{\mathcal{X}\mathcal{u}}\right]^{1/2}\left[1 + \frac{\mathcal{S}_v^{\,2}}{\mathcal{S}_y^{\,2}} + 2\frac{\mathcal{S}_v}{\mathcal{S}_y}R_{\mathcal{Y}\mathcal{v}}\right]^{1/2}} \tag{4.10}$$

In the case of dimensionless total energy $E_0^*$ and fetch $X^*$ scaled with wind velocity $\mathcal{U}_*$ as in (2.1) and (2.5), the correlation coefficient $R(\log E_0^*, \log X^*)$ is

$$R_{E_0^*X^*} = \frac{R_{E_0X} - 2\left(\frac{\mathcal{S}_{u_*}}{\mathcal{S}_X}\right)R_{E_0u_*} - 4\left(\frac{\mathcal{S}_{u_*}}{\mathcal{S}_{E_0}}\right)R_{Xu_*} + 8\frac{\mathcal{S}_{u_*}^2}{\mathcal{S}_X\mathcal{S}_{E_0}}}{\left[1 + 16\left(\frac{\mathcal{S}_{u_*}}{\mathcal{S}_{E_0}}\right)^2 - 8\left(\frac{\mathcal{S}_{u_*}}{\mathcal{S}_{E_0}}\right)R_{E_0u_*}\right]^{1/2}\left[1 + 4\left(\frac{\mathcal{S}_{u_*}}{\mathcal{S}_X}\right)^2 - 4\left(\frac{\mathcal{S}_{u_*}}{\mathcal{S}_X}\right)R_{Xu_*}\right]^{1/2}}. \quad (4.11)$$

In the limit when $\mathcal{S}_{E_0} \gg \mathcal{S}_u$ and $\mathcal{S}_X \gg \mathcal{S}_u$ then (4.11) implies

$$R_{E_0^*X^*} \approx R_{E_0X} \quad (4.12)$$

which is ideal in that there is no contamination of the dimensional correlation coefficient $R_{E_0X}$ by the variance $\mathcal{S}_{u_*}$. However, there is also no significant enhancement of the dimensionless correlation coefficient $R_{E_0^*X^*}$ due to contributions from $R_{E_0u_*}$ and $R_{Xu_*}$. This enhancement may generally be an objective in choosing scaling variables.

When $\mathcal{S}_{E_0} \approx \mathcal{S}_u$ and $\mathcal{S}_X \approx \mathcal{S}_u$, then

$$R_{E^*X^*} \approx \frac{R_{E_0X} - 2R_{E_0u_*} - 4R_{Xu_*} + 8}{[17 - 8R_{E_0u_*}]^{1/2}[5 - 4R_{Xu_*}]^{1/2}} \quad (4.13)$$

which does allow enhancement of $R_{E_0^*X^*}$ due to contributions from $R_{E_0u_*}$ and $R_{Xu_*}$. However, this is somewhat costly because in assuming $\mathcal{S}_{E_0} \approx \mathcal{S}_u$ and $\mathcal{S}_X \approx \mathcal{S}_u$ we are allowing considerable spuriousness. For example, if $R_{E_0u_*} \ll 1$ and $R_{Xu_*} \ll 1$ then $R_{E^*X^*}$ is almost 1.0. The relation for $R_{E^*X^*}$ is therefore quite insensitive to correlation between $E_0$ and $X$, as it becomes

$$R_{E_0^*X^*} \approx 0.108R_{E_0X} + 0.868. \quad (4.14)$$

It would be preferable to have $R_{E_0u_*}$ and $R_{Xu_*}$ contributions arise when $0 \ll R_{E_0u_*} \leq 1$ and $0 \ll R_{Xu_*} \leq 1$ but $\mathcal{S}_{E_0} \gg \mathcal{S}_u$ and $\mathcal{S}_X \gg \mathcal{S}_u$, which would be a subcase of the limit taken to obtain (4.12).

Finally if $\mathcal{S}_{E_0} \ll \mathcal{S}_{u_*}$, $\mathcal{S}_X \ll \mathcal{S}_{u_*}$, then

$$R_{E_0^*X^*} \approx 1.0 \quad (4.15)$$

which is completely spurious because $R_{E_0^*X^*}$ is essentially unity whether or not any of $\mathcal{U}$, $E_0$ or $X$ are correlated.

In Table 3 we present the correlation coefficients and variances that appear in (4.11) and we compute the ratio of $R_{E_0^*X^*}$ to $8\mathcal{S}_{u_*}^2(\mathcal{S}_X\mathcal{S}_{E_0})^{-1}$ as an inverse index of the relative contamination introduced into the dimensionless correlation coefficient due to $\mathcal{S}_{u_*}$. It is surprising that the ratio of $R_{E_0^*X^*}$ to $8\mathcal{S}_{u_*}^2(\mathcal{S}_X\mathcal{S}_{E_0})^{-1}$ is highest for scaling using $C_{d1}$, followed by $C_{d2}$ and finally $C_{d3}$, whereas in Table 2 we found that $R_{E_0^*X^*}$ was the same for scaling using $\mathcal{U}_*$ or $\mathcal{U}_{*c}$ for a given drag coefficient and was highest for scaling using $C_{d3}$, followed by $C_{d2}$ and finally $C_{d1}$. This ratio is also lower when $\mathcal{U}_{*c}$ rather than $\mathcal{U}_*$ is used in the scaling variable, implying that the variance of $\mathcal{U}_{*c}$ is higher than that of $\mathcal{U}_*$. While $\mathcal{U}_{*c}$ is marginally better at correlating with $X$ than $\mathcal{U}_*$, $\mathcal{U}_*$ clearly correlates better with $E_0$ than $\mathcal{U}_{*c}$, no matter which drag coefficient is used.

To consider the influence of $\mathcal{U}_*$ and $\mathcal{U}_{*c}$ on correlation coefficients of dimensionless variables, we use (4.10) to relate the dimensional correlation coefficients involving $E_0$ and $\mathcal{U}_*$ to those involving $E_0$ and $\mathcal{U}_{*c}$,

$$R_{E_0u_{*c}} = \frac{R_{E_0u_*} + \frac{\mathcal{S}_{\cos\Delta\theta}}{\mathcal{S}_{u_*}}R_{E_0}\cos\Delta\theta}{\left[1 + \left(\frac{\mathcal{S}_{\cos\Delta\theta}}{\mathcal{S}_{u_*}}\right)^2 + 2\frac{\mathcal{S}\cos\Delta\theta}{\mathcal{S}_{u_*}}R_{u_*\cos\Delta\theta}\right]^{1/2}} \quad (4.16)$$

and it is understood that, for example, $R_{E_0\cos\Delta\theta} = R(\log E_0, \log\cos\Delta\theta)$. The above analysis is con-

TABLE 3. The correlation coefficient for dimensionless total energy with fetch, as well as the correlation coefficients and variances which constitute it, and the ratio of $R_{E_0^*X^*}$ to $8\mathcal{S}_{u_*}^2[\mathcal{S}_X\mathcal{S}_{E_0}]^{-1}$ as an inverse index of the relative contamination due to $\mathcal{S}_{u_*}$, for winds within the ±30° window as in Table 2.

$R_{E_0X} = 0.519$, $\mathcal{S}_X = 0.320$, $\mathcal{S}_{E_0} = 0.387$

| | Scaling with $\mathcal{U}_*$ | | | Scaling with $\mathcal{U}_{*c}$ | | |
|---|---|---|---|---|---|---|
| | $C_{d1}$ | $C_{d2}$ | $C_{d3}$ | $C_{d1}$ | $C_{d2}$ | $C_{d3}$ |
| $\mathcal{S}_{u_*}/\mathcal{S}_X$ | 0.44 | 0.48 | 0.55 | 0.54 | 0.57 | 0.66 |
| $\mathcal{S}_{u_*}/\mathcal{S}_{E_0}$ | 0.36 | 0.40 | 0.46 | 0.45 | 0.47 | 0.54 |
| $R_{E_0u_*}$ | 0.719 | 0.738 | 0.658 | 0.537 | 0.581 | 0.515 |
| $R_{Xu_*}$ | −0.012 | 0.009 | −0.094 | −0.078 | −0.057 | −0.135 |
| $R_{E_0^*X^*}$ | 0.872 | 0.883 | 0.914 | 0.872 | 0.883 | 0.913 |
| $R_{E_0^*X^*}[8\mathcal{S}_{u_*}^2/\mathcal{S}_X\mathcal{S}_{E_0}]^{-1}$ | 0.688 | 0.575 | 0.452 | 0.449 | 0.412 | 0.320 |

TABLE 4. Variation of the correlation coefficients and variances constituting $R_{E_0 u_{*c}}$ as a function of the angle between wind direction and the direction of the dominant wave $|\Delta\theta|$; where winds are within ±30° of normal to the shoreline and $C_{d1}$ scaling is used.

| $\lvert\Delta\theta\rvert$ | $\mathcal{S}^2_{\cos\Delta\theta}$ ($\times 10^3$) | $\frac{\mathcal{S}_{\cos\Delta\theta}}{\mathcal{S}_{u_*}}$ | $R_{E_0\cos\Delta\theta}$ | $R_{u_*\cos\Delta\theta}$ | $R_{E_0 u_*}$ | $R_{E_0 u_{*c}}$ |
|---|---|---|---|---|---|---|
| 90° | 11.7 | 0.772 | −0.072 | −0.047 | 0.719 | 0.537 |
| 60° | 3.88 | 0.442 | −0.118 | −0.114 | 0.712 | 0.671 |
| 30° | 0.405 | 0.143 | −0.114 | −0.120 | 0.699 | 0.687 |
| 15° | 0.208 | 0.033 | −0.353 | −0.330 | 0.754 | 0.750 |

cerned with wind blowing from land to sea with the restriction that the angle between wind direction and the direction of the dominant wave satisfy $|\Delta\theta| \leq 90°$. Swell is separated from growing wind-sea as in Dobson et al. (1989) and results are shown in Table 4. It is evident that as $\Delta\theta$ is narrowed, $\mathcal{S}^2_{\cos\Delta\theta}$ decreases, $R_{E_0\cos\Delta\theta}$ and $R_{u_*\cos\Delta\theta}$ increase, $R_{E_0 u_{*c}}$ approaches $E_{E_0 u_*}$, and both increase. This increase in $R_{E_0 u_{*c}}$ and $R_{E_0 u_*}$ is not obvious because although the variance in $\mathcal{U}_{*c}$, $E_0$ and $\mathcal{U}_*$ decrease, the statistical population also decreases and therefore noise increases. Table 4 is for waves associated with the ±30° window from normal to the shoreline. Had this restriction been tightened to ±15°, the reduction of $\mathcal{S}^2_{\cos\Delta\theta}$ and the convergence of $R_{E_0 u_{*c}}$ to $R_{E_0 u_*}$ are still evident, as $\Delta\theta$ is decreased from ±90°. However, results are more subdued because the data population is smaller and the noise larger.

In Table 5 we present a reanalysis of the correlation coefficients and variances that appear in Table 3, with the restriction that the angle between wind direction and dominant wave direction $|\Delta\theta| \leq 15°$. The ratio of $R_{E_0^* X^*}$ to $8\mathcal{S}_{\mathcal{U}}{}^2(\mathcal{S}_X\mathcal{S}_{E_0})^{-1}$ is still highest for scaling using $C_{d1}$, followed by $C_{d2}$ and finally $C_{d3}$. However, $R_{E_0^* X^*}$ is the same for scaling using $\mathcal{U}_*$ or $\mathcal{U}_{*c}$ for a given drag coefficient. The variance of $\mathcal{U}_{*c}$ is now marginally lower than that of $\mathcal{U}_*$, while $\mathcal{U}_{*c}$ and $\mathcal{U}_*$ are essentially equivalent in terms of their ability to correlate with $X$ and $E_0$, no matter which drag coefficient is used. The ratio of $R_{E_0^* X^*}$ to $8\mathcal{S}_{\mathcal{U}}{}^2(\mathcal{S}_X\mathcal{S}_{E_0})^{-1}$ is now higher when $\mathcal{U}_{*c}$ rather than $\mathcal{U}_*$ is used in the scaling variable, for each choice of drag coefficient. This implies that reducing the variance of the scaling variable $\mathcal{U}_{*c}$, as we have done in the restriction $|\Delta\theta| \leq 15°$, reduces the contamination of the correlation coefficient due to self-correlation and makes $\mathcal{U}_{*c}$ preferable to $\mathcal{U}_*$ as the appropriate scaling variable.

In summary, we suggest that a proper treatment of the correlation coefficient of dimensionless variables $R_{\hat{X}\hat{Y}}$ must report the correlation coefficient of dimensional variables $R_{XY}$, and the latter must be significant. A discussion of the components that make up $R_{\hat{X}\hat{Y}}$ is possible from (4.10). Any enhancement of $R_{\hat{X}\hat{Y}}$ over $R_{XY}$ generally results from spurious self-correlation and from scaling variables that have a good physical basis. When a well-defined selection is made, for example, the CASP data with the restriction that the angle between wind direction and dominant wave direction $|\Delta\theta| \leq 15°$, better results follow from using physically motivated scaling variables. A more compelling demonstration would require data that is more free of noise. It is clear that we do introduce spurious self-correlation in scaling variables by a common factor, as in (2.3) and (2.6). Tables 3 and 5 show that simply using scaling variables with the highest values for $R_{\hat{X}\hat{Y}}$ ignores contamination due to spurious self-correlation.

## 5. Balance relations

### a. Total energy parameterization

Surface wave fields evolve in space and time according to the energy balance equation

$$\frac{\partial E}{\partial t} + \mathbf{V} \cdot \Delta E = S_{\text{in}} + S_{\text{nl}} + S_{\text{ds}} \qquad (5.1)$$

where $E(f, \theta; \mathbf{x}, t)$ is the two-dimensional wave spectrum; $\mathbf{V} = V(f, \theta)$ is the deep water group velocity; and $S_{\text{in}}$ is the energy input by the wind, $S_{\text{nl}}$ the nonlinear transfer due wave–wave interactions, and $S_{\text{ds}}$ the wave breaking dissipation. Refractive terms representing interaction with slowly varying currents, and dissipative bottom terms are not included in this discussion and are normally small.

Detailed energy balances are examined under various conditions by Komen et al. (1984), Hasselmann et al. (1985), Hasselmann and Hasselmann (1985) and Young et al. (1987). Rather than take this approach, we consider the basic large scale characteristics of wave generation dynamics following Resio and Perrie (1989). Therefore, denoting total energy $E_0$ where

$$E_0 = \int_0^{2\pi} \int_0^{\infty} E(f, \theta) df d\theta \qquad (5.2)$$

we are concerned with the rate of gain of total energy $\partial E_0/\partial t$ at a particular point on the sea surface.

When no swell is present, total wave energy is related to the shape of the spectrum and the location of the spectral peak. For an $f^{-4}$ equilibrium range, a dimensionally consistent spectral form is (1.5). Because $\psi$ and $\mathcal{J}$ are dimensionless in (1.5), we assume they are not strongly influenced by external parameters and that total energy can be represented as

$$E_0 = l\alpha^* g \mathcal{U}_* f_m^{-3} \qquad (5.3)$$

where $l$ is a dimensionless constant. This follows the

argument of Hasselmann et al. (1973) for an $f^{-5}$ spectrum. Inverting (5.3) gives the variation of $\alpha^*$ with $E_0$ and $f_m$.

Resio and Perrie (1989) considered the implications of an $f^{-4}$ equilibrium range for predicted growth patterns, the functional form of the input function due to wind $S_{in}$ and for the equilibrium range of the spectrum. JONSWAP fetch relations were assumed in their analysis. We present a new analysis within the context of the fetch relations found in the CASP data.

Given the energy fetch relation (3.1), the scaling implemented in (2.1) and (2.5) implies the corresponding dimensional relation

$$E_0 = \mathcal{E}\,\frac{\mathcal{U}_*^{4-2e}}{g^{2-e}}\,X^e \tag{5.4}$$

and the rate of change of total energy with fetch

$$\frac{\partial E_0}{\partial X} = \mathcal{E}\,\frac{\mathcal{U}_*^{4-2e}}{g^{2-e}}\,eX^{e-1}. \tag{5.5}$$

The wave studies of Kitaigorodskii (1962), Mitsuyasu (1968), Toba (1973) Hasselmann et al. (1973) and others show that wave spectra evolving with fetch tend to follow a self-similar pattern. Thus, any ensemble-averaged spectral function can be written as a dimensionless coefficient times the value at the spectral peak. For group velocity and phase velocity, this leads to

$$\left.\begin{aligned}\langle C_g\rangle &= \mathcal{B}_1\mathcal{C}_g\\ \langle C_p\rangle &= \mathcal{B}_2\mathcal{C}_p\end{aligned}\right\} \tag{5.6}$$

where $\mathcal{B}_1$ and $\mathcal{B}_2$ are dimensionless coefficients. Therefore, we write the fetch-limited time rate of growth as

$$\frac{\partial E_0}{\partial t} = \mathcal{B}_1\mathcal{C}_g\,\frac{\partial E_0}{\partial X} = \mathcal{B}_1\mathcal{C}_g\mathcal{E}\,\frac{\mathcal{U}_*^{4-2e}}{g^{2-e}}\,eX^{e-1}. \tag{5.7}$$

Equations (5.5) and (5.7) are fundamental relations for wave energy growth in terms of fetch and duration. For a given wind situation, equation (5.7) implies that total energy in the group velocity frame of reference increases at a decreasing rate as time evolves, if $e < 1$.

The corresponding rate of change of total momentum is

$$\frac{\partial M_0}{\partial t} = \frac{1}{\langle C_p\rangle}\,\frac{\partial E_0}{\partial t} = \frac{\mathcal{B}_1\mathcal{C}_{g_m}}{\mathcal{B}_2\mathcal{C}_{p_m}}\,\mathcal{E}\,\frac{\mathcal{U}_*^{4-2e}}{g^{2-e}}\,eX^{e-1}$$
$$\approx \frac{\mathcal{E}}{2}\,\frac{\mathcal{U}_*^{4-2e}}{g^{2-e}}\,eX^{e-1} \tag{5.8}$$

which implies that a decreasing proportion of momentum transfer from wind to water may be retained by the wave field provided $e < 1$ in (3.1).

### b. *Wind input spectral energy*

At present there is some uncertainty about the functional variation that the wind input $S_{in}$, should take. The consistency of the forms suggested by Plant (1982), Phillips (1985) and Snyder et al. (1981) is considered in Resio and Perrie (1989) assuming JONSWAP fetch relations. Following their approach, we partition an actively growing wave spectrum in Fig. 7a into three primary regions: "forward-face," "mid-range" and "high frequency" as a lowest order approximation. For most single peaked spectra, detailed numerical calculations show that net energy transfer due to wave–wave interactions may be described by three extrema, as presented in Fig. 7b, which approximately coincide with the regions of Fig. 7a. It follows that nonlinear transfers take energy from the midrange and give it to the forward face and the high frequency regions. As nonlinear transfers are conservative, energy taken from the midrange is equal to that gained by the other two regions.

Observed self-similarity in growing wave spectra leads us to assume that the main processes associated with growth are strongly related to the peak frequency location. Hasselmann et al. (1973) found from detailed numerical calculations that momentum transfers from midrange frequencies correspond approximately to constant proportions of momentum to lower frequencies where it is retained and to higher frequencies where it is dissipated. The equilibrium range and frequencies above the peak are approximately constant after the overshoot–undershoot phenomena has passed imply-

TABLE 5. As in Table 3 but with $|\Delta\theta| \leqslant 15°$.

$R_{E_0X} = 0.384$, $\mathcal{S}_X = 0.321$, $\mathcal{S}_{E_0} = 0.360$

| | Scaling with $\mathcal{U}_*$ | | | Scaling with $\mathcal{U}_{*c}$ | | |
|---|---|---|---|---|---|---|
| | $C_{d1}$ | $C_{d2}$ | $C_{d3}$ | $C_{d1}$ | $C_{d2}$ | $C_{d3}$ |
| $\mathcal{S}_{\mathcal{U}_*}/\mathcal{S}_X$ | 0.44 | 0.49 | 0.57 | 0.43 | 0.49 | 0.56 |
| $\mathcal{S}_{\mathcal{U}_*}/\mathcal{S}_{E_0}$ | 0.39 | 0.44 | 0.50 | 0.38 | 0.43 | 0.50 |
| $R_{E_0\mathcal{U}_*}$ | 0.754 | 0.781 | 0.713 | 0.750 | 0.778 | 0.709 |
| $R_{X\mathcal{U}_*}$ | −0.057 | −0.037 | −0.114 | −0.061 | −0.041 | −0.118 |
| $R_{E_0^*X^*}$ | 0.829 | 0.852 | 0.886 | 0.828 | 0.851 | 0.885 |
| $R_{E_0^*X^*}[8\mathcal{S}^2_{\mathcal{U}_*}/\mathcal{S}_X\mathcal{S}_{E_0}]^{-1}$ | 0.604 | 0.494 | 0.386 | 0.627 | 0.500 | 0.395 |

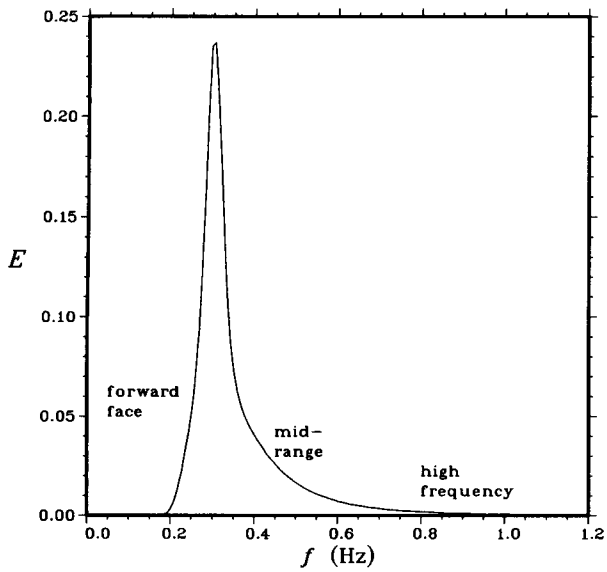


FIG. 7a. A single peaked wave spectrum showing the three regions: "forward-face", "midrange" and "high-frequency."

ing that the quasi-permanent retention of wave energy happens only at frequencies lower than the peak. This leads us to assume that the net gain of momentum on the forward face is approximately the net gain of momentum for the entire spectrum. In turn this is approximately a constant fraction of the momentum flux out of the mid-range frequencies which we estimate as

$$\frac{\partial M_m}{\partial t} = \frac{1}{p}\frac{\partial M_0}{\partial t} \tag{5.9}$$

where $p$ is a partitioning constant for the fraction of total momentum flux transferred from midrange frequencies to frequencies less than the spectral peak. For self-similarity within the spectrum, this momentum flux must be balanced by an input of momentum by the wind.

Denoting the input of momentum due to wind by $S'_{\text{in}}$, (5.8) implies

$$\int_{1.2f_m}^{2.5f_m} S'_{\text{in}}(f)df = \frac{1}{p}\frac{\partial M_0}{\partial t} \tag{5.10}$$

$$\approx \frac{1}{p}\frac{\mathcal{E}}{2}\frac{\mathcal{U}_*^{4-2e}}{g^{2-e}}\, eX^{e-1}. \tag{5.11}$$

In terms of the usual energy input due to wind, this may be written as

$$\int_{1.2f_m}^{2.5f_m} S_{\text{in}}(f)df \approx \mathcal{B}_2\mathcal{C}_p\frac{1}{p}\frac{\mathcal{E}}{2}\frac{\mathcal{U}_*^{4-2e}}{g^{2-e}}\, eX^{e-1} \tag{5.12}$$

which places a constraint on the functional form for $S_{\text{in}}$.

The Snyder et al. (1981) parameterization for wind input spectral energy may be generalized to the form

$$S_{\text{in}} \approx q_2\left(\frac{\mathcal{U}_*}{\mathcal{C}_p}\right)^n fE(f) \tag{5.13}$$

where $q_2$ is a dimensionless constant, and $n$ is to be determined. It is suggested by Snyder et al. (1981) that $n = 1$, whereas Phillips (1985) suggests, $n = 2$. From the spectral energy parameterization (1.5) we find

$$\int_{1.2f_m}^{2.5f_m} S_{\text{in}}(f)df \approx r_2\mathcal{U}_*^{n+1}\alpha^* f_m^{-2+n}g^{1-n} \tag{5.14}$$

where $r_2$ is a dimensionless constant. Equating this to the right side of (5.12) and rearranging terms, $\alpha^*$ may be related to $f_m^*$ and $X^*$:

$$\alpha^* = r_3(f_m^*)^{1-n}(X^*)^{e-1} \tag{5.15}$$

where $r_3$ is a dimensionless constant.

### c. *Equilibrium range constraints on spectral energy and $\alpha^*$*

An alternate way to derive the relationship for $\alpha^*$ is to consider the equilibrium range. The total energy flux from the central portion of the spectrum to high frequencies, parameterized in terms of integral properties of the spectrum and the location of the spectral peak may be written as

$$\Gamma_E = d_1\frac{E_0^3 f_m^9}{g^4} \tag{5.16}$$

where $d_1$ is a dimensionless constant. In terms of mo-

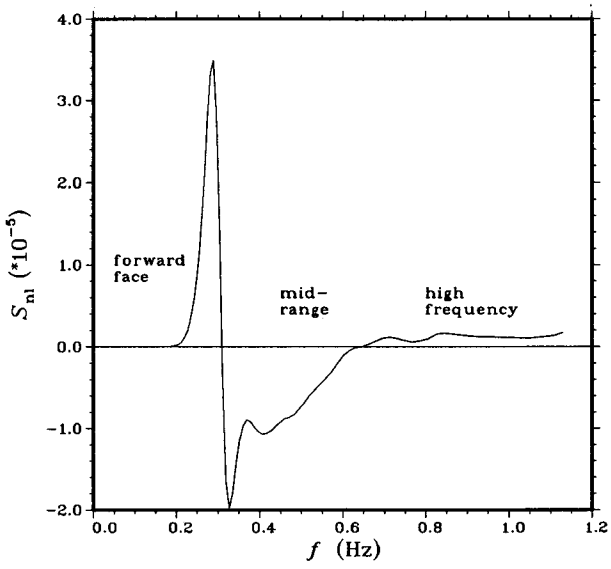


FIG. 7b. Nonlinear energy transfer due to wave–wave interactions showing three extrema which approximately coincide with the "forward-face", "midrange" and "high-frequency" regions.

mentum flux from mid-range frequencies to high frequencies this becomes

$$\Gamma_m = d_2 \frac{E_0^3 f_m^9}{f^4 \mathcal{C}_p} \tag{5.17}$$

where $d_2$ is a nondimensional constant.

Equation (5.17) describes the momentum flux to high frequencies due to nonlinear wave–wave interactions. We suppose that the energy input into the spectrum occurs within a somewhat localized domain and that an approximate balance between total momentum flux into the spectrum from the wind source and fluxes to higher and lower frequencies is

$$\tau_{\text{in}} \approx \tau_{ff} + \tau_{hf} \tag{5.18}$$

where $\tau_{\text{in}}$ is the net rate of momentum transfer from atmosphere to wave field, $\tau_{ff}$ is the rate of momentum transfer from the midrange frequencies to the spectral forward face and $\tau_{hf}$ is the rate of momentum transfer from the midrange frequencies to the high frequencies of the spectrum.

Following Hasselmann et al. (1973) and Resio and Perrie (1989), details of spectral shape are ignored and the proportion of total momentum flux from midrange to the forward face taken as a constant $Q$. We have

$$\tau_{ff} = Q\tau_{hf} \tag{5.19}$$

and by conservation of wave–wave interactions

$$\tau_{ff} + \tau_{hf} = (1 + Q)\tau_{hf} \approx \tau_{\text{in}}. \tag{5.20}$$

Therefore from Eqs. (5.11) and (5.17),

$$\tau_{\text{in}} = \frac{\partial M_m}{\partial t} \approx \frac{1}{p} \frac{\mathcal{E}\mathcal{U}^{4-2e}}{2g^{2-e}} e X^{e-1} \tag{5.21}$$

$$= (1 + Q) d_2 \frac{E_0^3 f_m^9}{g^4 \mathcal{C}_p} \tag{5.22}$$

and substituting equation (5.3) for total energy, $\alpha^*$ varies as

$$\alpha^* = \mathcal{A}(X^*)^{(e-1)/3}(f_m^*)^{-1/3} \tag{5.23}$$

where $\mathcal{A}$ is a nondimensional constant.

In Tables 6a and 6b, we compute the exponent $a$ in the fetch relation (3.3) for $\alpha^*$, using the energy normalization condition (3.14) and the CASP data. These are compared with the theoretical values specified by the total energy relation (5.3) and the equilibrium range expression (5.23). The most consistent determination of $\alpha^*$ and the maximum correlation coefficients $R$ for $\alpha^*$ occur when $\mathcal{U}_{*c}$ and $C_{d3}$ are used as scaling variables. This remains true when wave age is used as the independent variable.

The equilibrium range $\alpha^*$ relation (5.23) may be equated to the expression for $\alpha^*$ (5.15) derived as a consequence of the generalized Snyder et al. (1981) spectral wind input $S_{\text{in}}$. We infer the exponent $n$ of the generalized wind input

$$n = \frac{4}{3} + \frac{2(e-1)}{3e}. \tag{5.24}$$

Scaling with $C_{d3}$ and $\mathcal{U}_{*c}$, values of $n$ are computed to be about 1.3 whether $X^*$ or $\mathcal{U}_*/\mathcal{C}_p$ is used as the independent variable. Scaling with $\mathcal{U}_*$ and $C_{d1}$ implies that $n$ is about 2.0 as reported by Phillips (1985).

From the generalized relation for total wind input energy (5.14) and the Table 1 relation for $\alpha^*$ as a function of $\mathcal{U}_{*c}/\mathcal{C}_p$, we obtain

$$\int_{1.2f_m}^{2.5f_m} S_{\text{in}}(f)df \approx r_3 \mathcal{U}_{*c}^{2.3}(f_m^{*c})^{-0.67} f_m^{-0.7} g^{-0.3} \tag{5.25}$$

which may be rewritten as

$$\int_{1.2f_m}^{2.5f_m} S_{\text{in}}(f)df \approx r_3 \mathcal{U}_{*c}^{3}(f_m^{*c})^{-1.37} g^{-1}. \tag{5.26}$$

Using the wind input of Snyder et al. (1981) with $n = 1$ in (5.13) and the spectral energy parameterization of JONSWAP (1.1), the total wind input energy (5.14) is

$$\int_{1.2f_m}^{2.5f_m} S_{\text{in}}(f)df \approx r_4 \tilde{f}_m \tilde{\alpha} f_m^{-2} g^2. \tag{5.27}$$

Hasselmann et al. (1973) found in JONSWAP that

$$\tilde{\alpha} \approx 3.38(\tilde{f}_m)^{2/3} \tag{5.28}$$

which implies

$$\int_{1.2f_m}^{2.5f_m} S_{\text{in}}(f)df \approx r_5 \mathcal{U}^3(\tilde{f}_m)^{-1.33} g^{-1} \tag{5.29}$$

where $r_3$–$r_5$ are appropriate constants. This is consistent with (5.26) and confirms that total wind input energy has the same functional dependencies with either choice of scaling variables.

## 6. Concluding remarks

We have scaled the dimensional variables for wave spectra with the friction velocity magnitude $\mathcal{U}_*$, and also the friction velocity component $\mathcal{U}_{*c}$, in the direction of the waves at the peak frequency $f_m$. We have looked at three possibilities for the drag coefficient: $C_{d1}$ a constant, $C_{d2}$ the long-fetch open-ocean parameterization found by Smith (1988), and $C_{d3}$ the wave age dependent drag coefficient derived by Smith and Anderson (1989) in the HEXOS experiment for growing wind-generated waves.

Fetch relations exhibit a very large range of growth rates which generally support the slow variation in wave steepness with fetch found by Walsh et al. (1989). Scaling with $\mathcal{U}_{*c}$ and $C_{d3}$ was shown to exactly match their relation. The relations for total energy and peak frequency as a function of fetch depend on the scaling

TABLE 6a. Exponent $\alpha$ in fetch relation (3.3) is calculated from the energy normalization condition (3.14) in row 1, from the total energy relation (5.3) written as $\alpha^* = I_0 E_0^* (f_m^*)^3$ in row 2, and from the equilibrium range relation (5.23) in row 3. Assuming independent variable $\mathcal{U}_*/\mathcal{C}_p$, exponent $\zeta$ in fetch relation (3.12) is calculated as above, from energy normalization condition in row 4, from the total energy relation in row 5, and from the equilibrium range relation in 6. Correlation coefficients $R$ as well as comparative ratios to rows 1 and 4 are also presented. As in Table 1, the ±15° window is used.

| | | Scaling with $\mathcal{U}_*$ | | | Scaling with $\mathcal{U}_{*c}$ | | |
|---|---|---|---|---|---|---|---|
| Row | | $C_{d1}$ | $C_{d2}$ | $C_{d3}$ | $C_{d1}$ | $C_{d2}$ | $C_{d3}$ |
| 1 | $\alpha$ | 0.06 ± .05 | 0.08 ± .05 | 0.13 ± .05 | 0.12 ± .05 | 0.13 ± .05 | 0.17 ± .05 |
| | $R$ | 0.24 | 0.30 | 0.49 | 0.41 | 0.45 | 0.59 |
| 2 | $\alpha$ | 0.03 | 0.06 | 0.09 | 0.07 | 0.09 | 0.14 |
| | Percent of 1 | 50.0 | 75.0 | 69.2 | 58.3 | 69.2 | 82.4 |
| 3 | $\alpha$ | −0.003 | 0.007 | 0.07 | 0.05 | 0.057 | 0.113 |
| | Percent of 1 | −5.6 | 11.1 | 53.8 | 41.7 | 43.6 | 66.7 |
| 4 | $\zeta$ | −0.39 ± .19 | −0.43 ± .18 | −0.55 ± .15 | −0.59 ± .16 | −0.60 ± .16 | −0.67 ± .13 |
| | $R$ | −0.40 | −0.45 | −0.63 | −0.62 | −0.63 | −0.67 |
| 5 | $\zeta$ | −0.21 | −0.22 | −0.37 | −0.32 | −0.31 | −0.44 |
| | Percent of 4 | 53.8 | 51.2 | 67.3 | 54.2 | 51.7 | 65.7 |
| 6 | $\zeta$ | −0.031 | −0.071 | −0.258 | −0.210 | −0.230 | −0.372 |
| | Percent of 4 | 7.9 | 16.5 | 46.7 | 35.5 | 38.2 | 55.5 |

and the method of analysis. The dominating constraint is that, regardless of the method of analysis, wave steepness is almost invariant with respect to fetch.

In terms of duration- and fetch-limited growth, scaling variables imply a broad range of variation. For example, if the exponent on the fetch-limited relation for total energy (3.1) is greater than 1, the rate of change of total energy increases with time. If this exponent is less than 1, as we find in the CASP data scaling with $C_{d1}$ and $\mathcal{U}_*$ or as Donelan et al. (1985) found, the rate of change of total energy is decreasing.

The correlation coefficients for dimensionless variables $R_{\tilde{x}\tilde{y}}$ were related to the correlation coefficients among scaling variables, dimensional variables, and the variances of these variables. We suggest that a proper treatment of $R_{\tilde{x}\tilde{y}}$ must report the correlation coefficient of dimensional variables $R_{xy}$ and the latter must be significant. The situation where the scaling variables have a common factor $\mathcal{U}_*$ introduces spurious self-correlation to $R_{\tilde{x}\tilde{y}}$ and this self-correlation can be dominating. In the CASP dataset this effect can be reduced by choosing scaling variables that are well motivated and by selecting well defined data and scaling variables whose variances are low relative to the dynamical variables that are being scaled. These conditions were best met by restricting the angle between wind direction and the dominant wave direction to $|\Delta\theta| \leq 15°$ and scaling with $\mathcal{U}_{*c}$ rather than with $\mathcal{U}_*$.

Scaling with $\mathcal{U}_{*c}$ and $C_{d3}$ was shown to result in the greatest consistency among fetch relations in calculat-

TABLE 6b. As in Table 6a, but assuming ±30° window as in Table 2.

| | | Scaling with $\mathcal{U}_*$ | | | Scaling with $\mathcal{U}_{*c}$ | | |
|---|---|---|---|---|---|---|---|
| Row | | $C_{d1}$ | $C_{d2}$ | $C_{d3}$ | $C_{d1}$ | $C_{d2}$ | $C_{d3}$ |
| 1 | $\alpha$ | 0.07 ± .04 | 0.10 ± .05 | 0.15 ± .04 | 0.16 ± .04 | 0.17 ± .04 | 0.21 ± .04 |
| | $R$ | 0.21 | 0.29 | 0.44 | 0.44 | 0.47 | 0.59 |
| 2 | $\alpha$ | 0.05 | 0.07 | 0.12 | 0.11 | 0.10 | 0.15 |
| | Percent of 1 | 71.4 | 70.0 | 80.0 | 68.8 | 58.8 | 71.4 |
| 3 | $\alpha$ | 0.016 | 0.037 | 0.093 | 0.117 | 0.127 | 0.17 |
| | Percent of 1 | 22.9 | 37.0 | 61.2 | 73.1 | 74.7 | 81.0 |
| 4 | $\zeta$ | −0.42 ± .16 | −0.53 ± .15 | −0.61 ± .12 | −0.65 ± .11 | −0.69 ± .11 | −0.72 ± .09 |
| | $R$ | −0.34 | −0.44 | −0.57 | −0.63 | −0.65 | −0.73 |
| 5 | $\zeta$ | −0.19 | −0.25 | −0.36 | −0.35 | −0.36 | −0.45 |
| | Percent of 4 | 45.2 | 47.2 | 59.0 | 53.8 | 52.2 | 62.5 |
| 6 | $\zeta$ | −0.113 | −0.173 | −0.323 | −0.367 | −0.385 | −0.475 |
| | Percent of 4 | 26.9 | 32.6 | 53.0 | 56.5 | 55.7 | 65.0 |

ing $\alpha^*$, with respect to the CASP dataset. A parameterization of $\alpha^*$ derived from equilibrium range relations (5.23) was shown to verify well with $\alpha^*$ behavior in the total energy relation (5.3).

A generalization of the Snyder et al. (1981) parameterization for the spectral energy input to the waves by the wind was also suggested and evaluated in terms of the fetch relations. Whereas scaling by $\mathcal{U}_*$ and $C_{d1}$ implies that the $\mathcal{U}_*/\mathcal{C}_p$ term has an exponent of about 2.0 as reported by Phillips (1985), we demonstrate that scaling with $\mathcal{U}_{*c}$ and $C_{d3}$ implies an exponent of about 1.3. This is shown to lead to an expression for the total wind input energy consistent with that resulting from the Snyder et al. (1981) parameterization ($n = 1$) using the JONSWAP spectral parameterizations.

*Acknowledgments.* We have the pleasure of acknowledging many helpful conversations with Fred Dobson and Stu Smith. We are indebted to Ed Walsh for a valuable review of the manuscript. The wave modeling program at BIO is funded by the Federal Panel on Energy Research and Development (Canada).

## REFERENCES

Dobson, F., and B. J. Toulany, 1989: Wind-wave coupling. *The Johns Hopkins Tech. Digest.*

——, W. Perrie and B. Toulany, 1989: On the deep-water fetch laws for wind-generated surface gravity waves. *Atmos. Ocean,* **27**(1), 210–236.

Donelan, M. A., J. Hamilton and W. H. Hui, 1985: Directional spectra of wind-generated waves. *Phil. Trans. Roy. Soc. London,* **A315,** 509–562.

Hasselmann, K., T. P. Barnett, E. Bouws, H. Carlson, D. E. Cartwright, K. Enke, J. A. Ewing, H. Gienapp, D. E. Hasselmann, P. Kruseman, A. Meerburg, P. Müller, D. J. Olbers, K. Richter, W. Sell and H. Walden, 1973: Measurements of wind-wave growth and swell decay during the Joint North Sea Wave Project (JONSWAP). *Dtsch. Hydrogra. Z.,* Erganzungsheft Reihe A (8°), 12.

Hasselmann, S., and K. Hasselmann, 1985: Computation and parameterizations of the nonlinear energy transfer in a gravity wave spectrum. Part I: A new method for efficient computations of the exact nonlinear transfer integral. *J. Phys. Oceanogr.,* **15,** 1369–1377.

——, ——, J. H. Allender and T. P. Barnett, 1985: Computation and parameterizations of the nonlinear energy transfer in a gravity wave spectrum. Part II: Parameterizations of the nonlinear energy transfer for application in wave models. *J. Phys. Oceanogr.,* **15,** 1378–1391.

Janssen, P. A. E. M., G. J. Komen and W. J. P. de Voogt, 1987: Friction velocity scaling in wind wave generation. *Bound.-Layer Meteor.,* **38,** 29–35.

Jenkins, G. M., and D. G. Watts, 1968: *Spectral Analysis and its Applications,* Holden-Day.

Kenny, B. C., 1981: Beware of spurious correlations! *Water Resour. Res.,* **18**(4), 1041–1048.

Kitaigorodskii, S. A., 1962: Applications of the theory of similarity to the analysis of wind-generated wave motion as a stochastic process. *Bull. Acad. Sci.,* USSR Geophys. Ser. 1, 105–117.

Komen, G. J., S. Hasselmann and K. Hasselmann, 1984: On the existence of a fully developed wind-sea spectrum. *J. Phys. Oceanogr.,* **14,** 1271–1285.

Liu, P. C., and D. B. Ross, 1980: Airborne measurements of wave growth for stable and unstable atmospheres in Lake Michigan. *J. Phys. Oceanogr.,* **11,** 1842–1853.

Mitsuyasu, H., 1968: On the growth of wind-generated waves (I). *Rep. Res. Inst. Appl. Mech. Kyushu University,* **16,** 459–482.

Phillips, O. M., 1977: *The Dynamics of the Upper Ocean.* 2nd ed., Cambridge University Press, 366 pp.

——, 1985: Spectral and statistical properties of the equilibrium range in wind-generated gravity waves. *J. Fluid Mech.,* **156,** 505–531.

Plant, W. J., 1982: A relationship between wind stress and wave slope. *J. Geophys. Res.,* **87**(C3), 1961–1967.

Resio, D. T., and W. A. Perrie, 1989: Implications of an $f^{-4}$ equilibrium range for wind-generated waves. *J. Phys. Oceanogr.,* **19**(2), 193–204.

Smith, P. C., and J. I. McPherson, 1987: Cross-shore variations of near-surface wind velocity and atmospheric turbulence at the land-sea boundary during CASP. *Atmos.-Ocean,* **25,** 279–303.

Smith, S. D., 1988: Coefficients for sea surface wind stress, heat flux, and wind profiles as a function of wind speed and temperature. *J. Geophys. Res.,* **93,** 15 467–15 472.

——, and R. J. Anderson, 1989: Eddy flux measurements during HEXMAX. *Proc. NATO Advanced Workshop on Humidity exchange over the sea: Main experiment (HEXMAX) analysis and interpretation.* Tech. Rep. Dept. Atmos. Sci., University of Washington, HEXOS Contrib. No. 16.

Snyder, R. L., F. W. Dobson, J. A. Elliott and R. B. Long, 1981: Array measurements of atmospheric pressure fluctuations above surface gravity waves. *J. Fluid Mech.,* **102,** 1–59.

Taylor, P. A., and R. J. Lee, 1984: Simple guidelines for estimating wind speed variations due to small-scale topographic features. *Climatol. Bull.,* **18,** 3–32.

Toba, Y., 1973: Local balance in the air–sea boundary process III: On the spectrum of wind waves. *J. Oceanogr. Soc. Japan,* **29,** 209–220.

Walsh, E. J., D. W. Hancock, III, D. E. Hines, R. N. Swift and J. F. Scott, 1989: An observation of the directional wave spectrum evolution from shoreline to fully developed. *J. Phys. Oceanogr.,* **19,** 670–690.

Young, I. R., S. Hasselmann and K. Hasselmann, 1987: Computations of the response of a wave spectrum to a sudden change in wind direction. *J. Phys. Oceanogr.,* **17,** 1317–1338.